

Dynamic similarity promotes interpersonal coordination in joint-action

Piotr Słowiński¹, Chao Zhai², Francesco Alderisio², Robin Salesse³,
Mathieu Gueugnon³, Ludovic Marin³, Benoit G. Bardy^{3,4}, Mario
di Bernardo^{2,5,6}, and Krasimira Tsaneva-Atanasova^{1,6}

¹Department of Mathematics, College of Engineering, Mathematics
and Physical Sciences, University of Exeter, EX4 4QF, United
Kingdom

²Department of Engineering Mathematics, University of Bristol,
Merchant Venturers' Building, BS8 1UB, United Kingdom

³EuroMov, Montpellier University, 700 Avenue du Pic Saint-Loup,
34090 Montpellier, France.

⁴Institut Universitaire de France, Paris, France

⁵Department of Electrical Engineering and Information Technology,
University of Naples Federico II, 80125 Naples, Italy

⁶These authors contributed equally to this work

May 7, 2022

Abstract

Human movement has been studied for decades and dynamic laws of motion that are common to all humans have been derived. Yet, every individual moves differently from everyone else (faster/slower, harder/smoothier etc). We propose here a measure of such variability, namely an individual motor signature (IMS) able to capture the subtle differences in the way each of us moves. We show that the IMS of a person is time-invariant and that it significantly differs from those of other individuals. This allows us to quantify the dynamic similarity, a measure of rapport between dynamics of different individuals' movements, and demonstrate that it facilitates coordination during interaction. We use our measure to confirm a key prediction of the theory of similarity that the level of coordination between two individuals performing a joint task is higher if their motions share similar kinematic features. We evaluate the theory by applying it to the "mirror game", a recently proposed paradigm for studying the dynamics of two people improvising motion together. Moreover, we use a virtual avatar driven by an interactive cognitive architecture based on feedback control theory to

explore the effects of different kinematic features of the avatar motion on the coordination with human players.

Humans often need to perform joint tasks and coordinate their movement [1]. Their motion can be studied and classified by means of some common generalised movement laws [2, 3, 4] that define what it means to move in a “human-like” way [5, 6]. However, every individual moves following a specific personal style characterised by unique kinematic features. A pressing open problem is to find methods to capture such features and identify different individuals from the way they move. This is key to verify a central tenet of the theory of similarity in social psychology – that individuals moving in similar ways exhibit higher levels of coordination when performing joint tasks.

Specifically, studies of interpersonal interaction show that people prefer to interact with others who are similar to themselves [7, 8]. Moreover, it has been shown that social movement coordination between interacting people could be used to assess their mutual rapport [10, 11, 12]. These observations have led to the development of a theory of similarity which predicts that the level of coordination in joint actions is enhanced if the participants are similar in terms of morphology and movement dynamics and are willing to match their behaviours [13, 14, 15]. Despite previous attempts in the literature [16], this Ansatz has not been demonstrated with an adequate paradigm and via adequate variables.

In this paper we propose to go beyond the laws and principles that unify human movement, by deriving laws of individuality based on an *individual motor signature*. The individual motor signature notion has its roots in the frequency detuning (eigenfrequency difference) between two interacting humans and the so-called phenomenon of the maintenance tendency [17, 18, 19]. We focus here on identifying a more general and importantly time-invariant measure able to identify some key kinematic features of the motion of each individual and discriminate among different people. Using our measure, we are able to introduce a metric to assess the *dynamic similarity* between the movement of different humans and show that it predicts the level of human bonding in an interactive joint-action task.

We demonstrate the theory by using a virtual avatar playing the “mirror game”, an activity where two players are asked to imitate each other’s movements, and which has recently been established as a paradigm for studying collective movement dynamics (see [20, 21] and references therein).

Our evidence shows that similarity between the preferred motion of each player enhances the coordination level measured during the interaction thus confirming the predictions of the theory of similarity.

More generally, our research establishes the foundations of a new approach to studying dynamic similarity as an important factor affecting joint actions and enhancing coordination between socially interacting people.

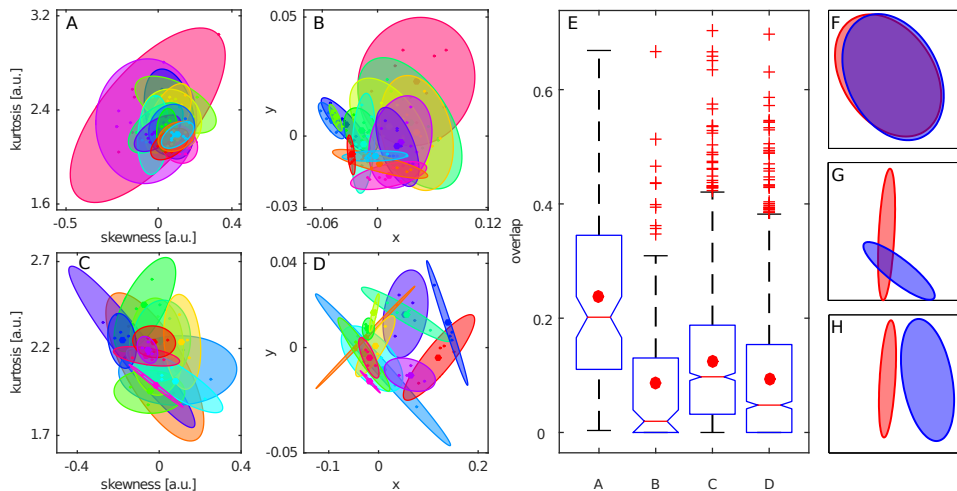


Figure 1: Individual motor signature in A the kurtosis-skewness of velocity segments plane [20] and in B the *similarity space* computed with MDS from distances between velocity profiles. For 15 different participants from experimental Scenario 1 (see *Materials and methods*), on three different days with at least one week break between recording rounds. Positive velocity segments and velocity profiles from 56 solo trials of 14 participants from experimental Scenario 3 (see *Materials and methods*) shown in C the skewness-kurtosis plane and in D the *similarity space* (for the sake of clarity data for only 14 out of 53 participants is shown). Different colours corresponds to different participants. Small dots correspond to individual solo recordings. Each big dot at the centre of an ellipse corresponds to the average of the small dots' positions. Each ellipse indicates 0.7 mass of bivariate normal distribution fitted to the small dots (see *SI appendix* for further details). Box plots in panel E show distributions of overlaps ω between pair of ellipses in panels A–D. Red line indicates median, red dot indicates mean. The "central box" represents the central 50% of the data and its lower and upper boundary lines are at the 25%/75% quantile of the data. The two vertical lines extending from the central box indicate the remaining data outside the central box that are not regarded as outliers, red crosses indicate outliers. Panels F–G show examples of overlap ω between pair of ellipses: F the ellipses almost completely overlap, $\omega=0.93$; G the ellipses partially overlap, $\omega=0.13$; H the ellipses do not overlap, $\omega=0$.

1 Results

1.1 Existence of an Individual Motor Signature

Before studying the effect of dynamic similarity on coordination during an interactive task, it is necessary to demonstrate that: 1) every individual's

movements are characterised by specific kinematic properties that can be used to define an individual motor signature, and 2) the movement characteristics (i.e. the motor signature) of each individual persist in time. To this end, 15 participants were asked to perform a solo movement in the mirror game (in the absence of any other player) on 3 different days with at least one week break between experimental sessions; as described in *Materials and methods*, Scenario 1.

Following [20] we began our analysis by studying kurtosis and skewness of velocity segments. Velocity segments, which were used to analyse the mirror game in [20, 21, 28], are parts of the velocity time series where the participant is moving in one direction, i.e., parts of the velocity time-series between two consecutive times of zero velocity. From the viewpoint of motion dynamics, skewness indicates asymmetry in acceleration and deceleration, while kurtosis provides information about uniformity of the maximal velocity in a velocity segment. Low kurtosis indicates that an object was quickly accelerating and decelerating, and kept maximal velocity for a long time. High kurtosis, on the contrary, means that the object was accelerating slowly, and moved with maximal velocity only for a short period of time. Our analysis revealed that, despite being a good source of information about human movement on a short time-scale (rates of acceleration, uniformity of maximal velocity), velocity segments are not specific enough to study the effects of dynamic similarity between individual players. More specifically, we find that although the mean values of kurtosis and skewness of velocity segments exhibit clustering for each person, and that the clusters are preserved over time, there also exists a big overlap between mean skewness and kurtosis of different players, meaning that it is not possible to distinguish between them; see Fig. 1A, C and E. In particular, such overlap can be quantified by $\omega \in [0, 1]$, where $\omega = 0$ corresponds to no overlap and $\omega = 1$ to total overlap (see SI appendix for further details).

Therefore, we analysed instead velocity profiles (probability density functions (PDFs) of the frequency distributions based on velocity time series as described in *Materials and methods*) which characterise motion in the mirror game on the time-scale of a complete experimental trial. We used the Earth Mover’s Distance (EMD) to assess distances between velocity distributions computed on the movement trajectories of different individuals (as described in *Materials and methods*). We then projected them onto the *similarity space*, that is an abstract geometric space constructed by means of multidimensional scaling (MDS) [27] that provides a visual representation of the pattern of proximities (i.e., similarities or distances) among a set of objects (see *Materials and methods* for further details). We were able to reveal that the coordinate x of the movement representation in the *similarity space*, which corresponds to the first principal dimension given by the MDS, is correlated with the amount of high frequency components in the movement measured as a power in the 1.5-10 [Hz] band, i.e it carries information

about maximal velocities as high frequencies indicate faster movement. Also, the y coordinate of the representation of each time series in the *similarity space*, which corresponds to the second principal dimension from the MDS, is correlated with the kurtosis, that is the normalised form of the fourth curve moment of the velocity segments [20, 21], i.e. it informs us on the ratio of high and low velocities in a typical velocity segment.

For further details see: *SI appendix* Fig. 10 and Table 3.

Figure 1B depicts velocity profiles of individual players presented as elements of the *similarity space*. Figure 1E clearly demonstrates that the median overlap $\tilde{\omega}$ between ellipses, and hence individuals, in the skewness-kurtosis plane $\tilde{\omega}_A = 0.2$ is much higher than the median overlap between ellipses in the *similarity space* $\tilde{\omega}_B = 0.02$ (significance $p_{AB} < 0.0001$, Kolmogorov-Smirnov test [29, 42]). More importantly, there are 45 out of 105 pairs of ellipses that do not overlap at all in the *similarity space* while in the kurtosis-skewness plane all pairs of ellipses overlap, ($\min \omega_A = 0.004$). To verify our results we also analysed solo recordings collected in the experimental Scenario 3; see Fig. 1C and D. In the experimental Scenario 3, players had larger range of movement and all the solo trials of individual players were recorded on a single day; see *Materials and methods*, Scenario 3. Nevertheless in this case we also find that the median overlap $\tilde{\omega}$ between ellipses in the skewness-kurtosis plane $\tilde{\omega}_C = 0.1$ is much higher than the median overlap between ellipses in the *similarity space* $\tilde{\omega}_D = 0.05$ (significance $p_{CD} < 0.0001$) and the number of non-overlapping pairs of ellipses is higher in the *similarity space* (418 against 183 out of 1378 pairs). In both experimental scenarios, we observe that separation between ellipses, and hence individuals, is significantly better in the *similarity space*.

In view of the above analysis, we propose to define the *individual motor signature* (IMS) of a person in terms of the aggregate properties (depicted as ellipses in Figure 1B) of a collection of velocity profiles of her/his solo recordings in the similarity space. Postulated in this way, individual motor signatures identify each different participant and can be used effectively to measure dynamic similarity between them. Furthermore they provide a comprehensive and holistic description of the kinematic characteristics and variability of human movement compared to the skewness and kurtosis of velocity segments.

An interesting additional observation concerns the variability between radii of the ellipses associated with different individuals and their dimensions. Smaller ellipses indicate a greater time-invariance of the IMS over different trials whereas bigger ellipses signify that the IMS of that individual is more variable over time (Fig. 1B and D).

Using the concept of IMS as defined in the similarity space, we were able to demonstrate the plasticity of individual motor signatures during social interaction. Indeed, we found that some people are more inclined to adjust their kinematic characteristics when interacting with others in the

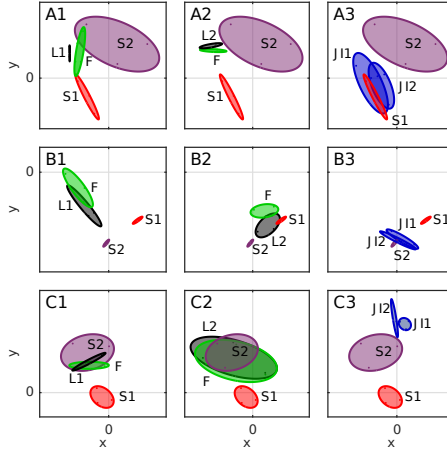


Figure 2: Interaction between two players in different experimental conditions visualised in the *similarity space*. Ellipses encircle points corresponding to velocity profiles in solo (S; red and purple), leader (L; black), follower (F; green) and joint improvisation (JI; blue) rounds. Each row depicts data for a different dyad. In column 1 player 1 was a leader, in column 2 player 2 was a leader and in column 3 participants played in joint improvisation condition. x axis has the same range in all panels, y axis is rescaled for clarity of presentation.

mirror game. Figure 2 shows three representative examples of motor signature plasticity detected during the experiment described in *Materials and methods*, Scenario 2. In Fig. 2A1 and A2 we observe the same consistent behaviour of the leader and follower independently of which player is the designated leader. In Fig. 2B1 and B2 we notice that dynamics of movement differs significantly depending on who is leading. In Fig. 2C1 and C2 we observe that player 2 dominates the interaction in terms of movement dynamics. Furthermore, Figure 2A3–C3 clearly shows that motion dynamics in the joint improvisation condition is different than in the leader-follower condition. More generally, Fig. 2 demonstrates that the relationship between individual motor signatures in solo movement and movements during cooperative conditions are rather complex and consistent with the analysis based on velocity segments collected in cooperative conditions, reported in [20, 30]. Taken together the above observations suggest that individual motor signatures might be regulable rather than fixed and could be modulated in order to enhance social competence.

1.2 Dynamic similarity enhances coordination in joint action

In order to analyse the dependence of the coordination level on the dynamic similarity, we measure the temporal correspondence between players in the

mirror game and study systematically if and how it is related to the difference between their individual motor signatures. To this end, we analysed the effects of the dynamic similarity on the temporal correspondence in two different experimental scenarios: the former where two humans play the mirror game and the latter where a human is asked to play the game with a virtual player (VP or avatar). The VP is driven by an interactive cognitive architecture (ICA) and is able to play the game with a human player while exhibiting some desired dynamic movement properties [35, 36].

In order to generate the trajectory of the VP’s movement, pre-recorded position time series from solo trials of human players were used as input data for the ICA. We shall refer to such trajectories as the VP’s reference trajectories (Ref). The ICA uses an adaptive feedback control algorithm to generate the VP’s movement while being influenced by the follower’s performance (see [35, 36] for further details). It is important to note that the ICA does not simply replay pre-recorded time-series as in [28], but uses them as preference signal in order to generate the output trajectory for the VP. This allows for a real-time movement behaviour matching between participants, which is a fundamental part of the interaction in the mirror game. For instance, if the follower stops tracking the movement of the leader, it is appropriate for the leader, as done by the ICA driving the VP, to adjust its movement and guide the follower in order to encourage the interaction.

In the experiments, each player was asked to follow the VP fed with two different reference trajectories: 1) in the similar condition, the player’s own solo movement was used as the Ref; and 2) in the dissimilar condition, a 2.5Hz sinusoidal signal was superimposed to the same solo trajectory, with time varying amplitude defined as 1/3 of the corresponding normalised velocity. In all trials, the non-adaptive parameters of the ICA were kept at fixed values (See *SI appendix* for further details). We measured temporal correspondence between players by means of the *relative error in position* (RPE). The RPE is a measure of temporal correspondence between complex, non-periodic, coordinated movements which is based on the natural notion of a follower lagging behind the leader when tracking her/his motion (See *Materials and methods* for further details). Comparison to other measures of coordination can be found in *SI appendix*.

In order to demonstrate that dynamic similarity facilitates coordination between players in the mirror game we seek to find a correlation between dynamic similarity, as quantified by means of the distance between velocity profiles in the similarity space, and temporal correspondence measured by the RPE. Fig. 3A–C illustrates the steps we take in our analysis detailed in the figure legend. The correlation between temporal correspondence and dynamic similarity observed in the data from human-human interaction collected in the experimental Scenario 2 is shown in Fig. 3D. For each dyad we calculate nine values for the distance between the players signatures S_1 and S_2 (all the combinations between three solo trials for each player) and six

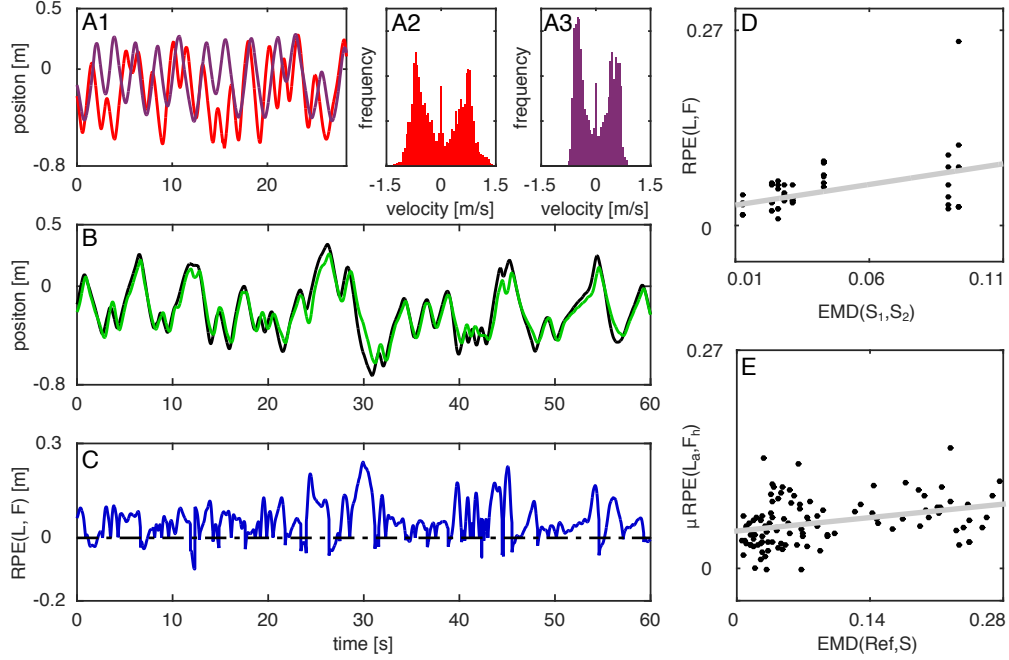


Figure 3: First we compute dynamic similarity between two players. In panel A1 we show the solo movements of two participants (S_{A2} and S_{A3}) who later played together in the leader-follower condition. Panels A2 and A3 depict individual motor signatures (IMS) of the two players corresponding to the positions time series presented in panel A1. The $EMD(S_{A2}, S_{A3}) = 0.0303$ between the histograms in panels A2 and A3 quantifies dynamic similarity between the two players. Then we measure temporal correspondence between their movements when they play together in the leader-follower condition. Panel B illustrates position traces of the participants from panel A when they play together as a leader (black) and follower (green). Panel C shows the RPE between leader and follower trajectories presented in panel B. The mean value and the standard deviation of the RPE are respectively $\mu RPE(L_{A2}, F_{A3}) = 0.05$ and $\sigma RPE(L_{A2}, F_{A3}) = 0.05$. Panel D shows correlation between $EMD(S_1, S_2)$ and $RPE(L, F)$ computed for all individual leader-follower trials in 8 dyads from Scenario 2 (each black dot corresponds to a single leader-follower trial). Panel E depicts the dependence of mean $\mu RPE(L_a, F_h)$ of RPE between the VP leading the human participant on $EMD(Ref, S)$ between the reference trajectory and the participant's solo movement.

values for the mean RPE between leader (L) and follower (F) (three trials with player 1 as a leader and three trials with player 2 as a leader); Spearman's rank correlation [31, 42] between distance and RPE was computed to

be $\rho=0.4371$ ($p_\rho=0.0019$).

We confirmed our observations by also analysing data from the experimental Scenario 3, where a VP leads a human follower. In particular, we computed correlations between the similarity of the two players (evaluated in terms of the distance between the velocity profile of the avatar reference trajectory and that of the preferred motion of the human player) and their temporal correspondence.

Figs. 3E demonstrates that temporal correspondence depends on the dynamic similarity between the reference trajectory of the VP and participant's solo movement. In particular, comparing a VP (avatar) leader (L_a) and a human follower (F_h) we find that mean and standard deviation of the RPE between leader and follower increase with the distance between their signatures, which affirms that dynamic similarity between reference trajectory and player's solo movements facilitates temporal correspondence between the VP leader and human follower. To statistically confirm this Ansatz, we used Spearman's rank correlation test; all correlation coefficients can be found in *SI appendix*, Tab. 1.

In summary, we show that a small distance between individual velocity profiles of the leader and the follower, indicating that they have similar movement dynamics, results in higher levels of coordination than those observed in dyads in which the distance between participants' individual motor signatures is larger. In so doing, we reveal that dynamic similarity governs the level of coordination in joint human movement interactions and confirm the key prediction of the theory of similarity that dynamic similarity enhances inter-human interaction.

2 Conclusions

In this paper we introduced the notion of dynamic similarity in the mirror game [21] and demonstrated the existence of an individual motor signature in human players. We then showed that the coordination level between the players is affected by their dynamic similarity.

In particular, we proposed the use of velocity profiles, defined by the probability density functions of velocity time series recorded in the mirror game, as motor signatures. We used the earth's mover distance (EMD) and multidimensional scaling (MDS) to show that velocity profiles of the solo movement have characteristics of individual motor signatures, i.e. they are stable over time and differ significantly between individual players. In this way we revealed time-persistent, individual motor properties that could be detected in complicated, non-periodic motion observed in the mirror game, as suggested in [20]. Notably we extended the notion of motor signature beyond the frequency content of a periodic motion [17, 18, 19, 32]. Existence of individual motor signatures allowed us to validate dynamics of motion as

an important element of the theory of similarity along side individual’s morphology and behaviour. Since the individual motor signature can be readily recorded by means of cheap off-the-shelf experimental set-up, we believe that it could become an integral part of studies investigating interpersonal interaction.

We introduced the evaluation of the distance between velocity profiles as a method of quantifying dynamic similarity between players’ motion in the mirror game and the use of the relative position error (RPE) to measure their temporal correspondence. Our key finding confirms the central predictions of the theory of similarity, namely that dynamic similarity of participants’ solo motions enhances their coordination level [19, 38].

Finally, the methods we have introduced and the data we have collected establish the use of a virtual player (VP) [39], driven by an interactive cognitive architecture (ICA), as an effective tool for studying joint actions in the mirror game, and to show that human-avatar interaction offers a flexible and effective approach to studying interactions between humans. Importantly, the advantages of using an interactive cognitive architecture based on feedback control to drive the avatar is that bi-directional coupling is maintained during the mirror game and that it allows control of the interaction between human and avatar in two ways, both by choosing reference trajectories and by changing the bi-directional coupling parameters of the ICA. Such level of control on movement coordination could be used to reinforce social bonding in joint-action tasks [11, 40].

3 Materials and Methods

3.1 Experimental Setup and Data Collection

The results presented in this paper are based on the analysis of data collected in three different experimental scenarios, performed in the course of the research project AlterEgo funded by the European Union [33]. In Scenario 1 we only collected solo movements of the participants; in Scenario 2 we collected data from humans playing the mirror game in a solo condition and in dyads; in Scenario 3 we collected data from human participants playing solo and interacting with a virtual player (VP).

3.2 Scenario 1

Data in Scenario 1 was collected by means of a set-up consisting of a leap motion device [34] and a laptop (more details on the leap motion setup can be found in *SI appendix*). Each participant was asked to sit comfortably on a chair and create interesting motion by moving her/his preferred hand above the leap motion sensor. Participants were given the following instruction: “Play the game on your own, create interesting motions and enjoy playing”.

The movement of a participant was visualised on the screen of the laptop as a dot. Due to the nature of the experimental set-up, the position was recorded in arbitrary units. We asked 15 participants to perform three solo sessions, each one separated by at least one week. At each session, a participant was required to perform three solo rounds, each one lasting 60 seconds. In total, we recorded nine position time series for each participant.

3.3 Scenario 2

In Scenario 2 participants sat comfortably opposite each other. Two horizontal strings (length 1800mm) were mounted at eye level, centrally between the participants; on each string a ball with a small handle was mounted. Participants were instructed to move these balls left and right along the strings during the experiment. The movements of each participant were captured using reflecting marker placed on the ball with infrared MX13 cameras (Vicon-Nexus, Oxford Metrics Ltd.) at a sampling rate of 100 Hz. Data was collected from 8 dyads (16 participants in total). All participants were right handed. Participants were given the following instructions:

- Solo Condition. Participants were given the same instruction as in Scenario 1. Participants had no view of their partner.
- Leader-Follower Condition. “This is a collaborative round whose purpose is to enjoy creating synchronised motion. Participant 1, lead the movement. Participant 2 try to follow your partner’s movement.” Two versions of this condition were played to allow both participants to lead and to follow.
- Joint Improvisation Condition. “In this collaborative round there is no leader and no follower. Let these 2 roles emerge naturally, imitate each other and create synchronised and interesting motions. Enjoy playing together.”

3.4 Scenario 3

In Scenario 3, human players were asked to play with the VP driven by the interactive cognitive architecture presented in [35, 36]. Participants were standing in front of an LCD display showing the VP. A horizontal string (length 1800mm) was mounted in front of the participant. As previously, a ball with a small handle was mounted on the string. Participants were instructed to move the ball left and right along the string. On the screen facing the human player, the VP was also moving a ball along a string. The movement of each participant was recorded with a single wide-angle camera. The sampling rate was not uniform and averaged around 40Hz.

In order to verify that the interactive cognitive architecture, having as an input different types of reference trajectories, could generate movements

with different dynamics, we computed EMDs between VP leader movements in similar (players solo movement) and dissimilar conditions (players solo movement + 2.5 Hz sine). The mean EMD between velocity profiles of leader’s movements generated with similar and dissimilar reference trajectory is 0.0140. This confirms that the leader’s movements generated by the ICA in these two conditions, using different types of reference trajectories, had different dynamic characteristics.

Data was collected from 53 individuals playing the mirror game with the VP. The data set of each participant contained positions for each of the following rounds:

- 4 solo (one minute) rounds. One of the solo recordings was used as a reference trajectory for the ICA.
- 12 rounds (one minute) where the human participant plays as the leader.
- 12 rounds (30 seconds) where the human participant plays as a follower in similar condition and 12 rounds (30 seconds) as a follower in dissimilar condition.
- 24 displayed position time series (30 seconds) of the VP leading the human participant.
- 1 (one minute) reference trajectory used in the dissimilar condition.

3.5 Data pre-processing

The collected data was pre-processed in Matlab. When necessary we used interpolation with shape-preserving piecewise cubic interpolation and filtering with a zero-phase forward and reverse digital 2nd order lowpass (10Hz cut-off) Butterworth filter. For further details see *SI appendix*.

3.6 Velocity profiles

The pre-processed position time series were used to numerically estimate their corresponding velocity time-series. To differentiate position time-series we used a forth-order finite difference scheme. We cut out the first and last 2 seconds of the signal. Furthermore, we limited velocities to 3.5 [a.u./s] in the experimental Scenario 1 and to 2.7 [m/s] in the experimental Scenarios 2 and 3 (higher velocities were considered as results of noise in the collected data). To estimate the PDF of the player’s velocity we use normalised histogram of the velocity time series with 101 equally distant bins between -2.7 and 2.7 [m/s] (or -3.5 and 3.5 [a.u./s] in Experiment 1). For further details see *SI appendix*.

3.7 Earth’s movers distance

Mathematically the EMD is a special case of Wasserstein distance [25]. It is a solution of the optimal transportation problem [37] and is an established tool in image analysis and pattern recognition applications [25]. For univariate PDFs it can be expressed in a closed form as the area between their corresponding cumulative distribution functions [24]:

$$\text{EMD}(PDF_1(z), PDF_2(z)) = \int_Z |CDF_1(z) - CDF_2(z)| dz$$

Here, PDF_1 and PDF_2 are two probability density functions with support in set Z , CDF_1 and CDF_2 are their respective cumulative distribution functions. In practice, to compute empirical CDFs we take the cumulative sum of histogram bins normalised by the number of data points. We use histograms with 101 equidistant bins over fixed range of velocity values (outliers are assigned to the most extreme bins). Furthermore, we normalise the EMDs with the maximal EMD for a given support Z ; since $|CDF_1(z) - CDF_2(z)| \leq 1$, the maximal EMD is given by the length of the support $\text{EMD}_{max} = |Z|$. See more details in *SI appendix*.

3.8 Multidimensional scaling

Multidimensional scaling is a well established tool in data visualisation and data mining [27]. It allows to reduce dimensionality of the data and visualise relations between the objects under investigation while preserving as much information as possible. Since the EMD is a metric in the space of velocity profiles (defined by the PDFs of velocity time series), we use classical MDS as implemented in Matlab. See more details in *SI appendix*.

3.9 Relative position error

The RPE is based on the notion that if two objects are moving in the same direction then the one behind is following, and on the assumption that changes of direction of movement are initiated by the leader. We define the RPE as the difference in the players’ positions multiplied by their common direction of motion. In cases when the players are moving in opposite directions, we assume that the follower is always behind the leader, regardless of directions of players’ movement. These rules lead to the following formula for computing the $\text{RPE}(x_1(t), x_2(t))$:

$$\begin{cases} (x_1(t) - x_2(t)) \text{sgn}(v_1(t)), & \text{sgn}(v_1(t)) = \text{sgn}(v_2(t)) \neq 0, \\ |x_1(t) - x_2(t)|, & \text{otherwise.} \end{cases}$$

Here x_1, v_1 are position and velocity of the leader and x_2, v_2 are position and velocity of the follower. Positive values of the RPE mean that the follower is behind the leader. We note that the RPE is not symmetric, that is

$\text{RPE}(x_1(t), x_2(t)) \neq -\text{RPE}(x_2(t), x_1(t))$ (due to the assumption that a follower should react to the action of a leader) and therefore, it could be treated as a measure of the performance of the follower in addition to indicating the level of temporal correspondence (coordination). Such interpretation of the RPE is consistent with the fact that the mismatch in position is one of the control parameters of the interactive cognitive architecture. Further details can be found in the *SI appendix*.

Acknowledgments

The authors would like to thank Ed Rooke (University of Bristol), Catherine Bortolon (University Hospital of Montpellier) and Zhong Zhao (University of Montpellier I) for help in data collection, as well as preparing and running some of the experiments. We would also like to thank Richard Schmidt and Michael Richardson for helpful discussions.

This work was funded by the European Project AlterEgo FP7 ICT 2.9 - Cognitive Sciences and Robotics, Grant Number 600610. The research of KT-A was supported by grant EP/L000296/1 of the Engineering and Physical Sciences Research Council (EPSRC).

References

- [1] Schmidt, R.C., Richardson, M.J.: (2008) Coordination: Neural, behavioral and social dynamics. In: Coordination: Neural, behavioral and social dynamics. Springer: 281–308.
- [2] Hogan, N., Flash, T.: (1987) Moving gracefully: quantitative theories of motor coordination. Trends in Neurosciences 10:170–174.
- [3] Viviani, P., Flash, T.: (1995). Minimum-jerk, two-thirds power law, and isochrony: converging approaches to movement planning. Journal of Experimental Psychology: Human Perception and Performance, 21(1), 32.
- [4] Hogan, N., Sternad, D.: (2007) On rhythmic and discrete movements: reflections, definitions and implications for motor control. Exp Brain Res 181:13–30.
- [5] Kilner, J.M., Paulignan, Y., Blakemore, S.J.: (2003). An Interference Effect of Observed Biological Movement on Action. Current Biology, 13(6), 522-525
- [6] Kilner, J., Hamilton, A. F. d. C., Blakemore, S.J.: (2007). Interference effect of observed human movement on action is due to velocity profile of biological motion. Social Neuroscience, 2(3-4), 158-166.

- [7] Folkes V.S.: (1982) Forming relationships and the matching hypothesis. *Personality and Social Psychology Bulletin*, 8 (4):631–636.
- [8] Marsh, K.L., Richardson, M. J., Schmidt, R.: (2009) Social connection through joint action and interpersonal coordination. *Topics in Cognitive Science*, 1(2), 320–339.
- [9] Kelso, J. S. (1997). *Dynamic patterns: The self-organization of brain and behavior*: MIT press.
- [10] Lakens, D., Stel, M.: (2011) If they move in sync, they must feel in sync: Movement synchrony leads to attributions of rapport and entitativity. *Social Cognition*, 29(1): 1–14.
- [11] Oullier, O., De Guzman, G. C., Jantzen, K. J., Lagarde, J., Kelso, J. S.: (2008) Social coordination dynamics: Measuring human bonding. *Social neuroscience*, 3(2): 178–192.
- [12] Schmidt, R.C., Nie L., Franco A., Richardson, M.J.: (2014) Bodily synchronization underlying joke telling. *Front. Hum. Neurosci.* 8:633. doi: 10.3389/fnhum.2014.00633
- [13] Pinel, E. C., Long, A. E., Landau, M. J., Alexander, K., Pyszczynski, T.: (2006) Seeing I to I: a pathway to interpersonal connectedness. *Journal of Personality and Social Psychology*, 90(2), 243.
- [14] Bardy, B. G., Salesse, R. N., Gueugnon, M., Zhao Zhong, Lagarde, J., Marin, L.: (2014) Movement similarities and differences during social interaction. *IEEE International Conference on Systems, Man and Cybernetics (SMC)*, 772–777.
- [15] Zhao, Z., Salesse, R. N., Gueugnon, M., Schmidt, R. C., Marin, L., Bardy, B. G.: (2015) Moving attractive virtual agent improves interpersonal coordination stability. *Human Movement Science*, 41, 240-254.
- [16] Qin, J., O’Meara, B., McEachern S.: (2009) The need for an integrated theoretical framework for researching the influence of group diversity on performance, *Management Research News*, vol. 32, pp. 739-750.
- [17] von Holst, E.: (1973) *The behavioral physiology of animal and man*. Coral Gables, FL: University of Miami Press. (Original work published 1939)
- [18] Rosenblum, L. D., Turvey, M.: (1988) Maintenance tendency in coordinated rhythmic movements: Relative fluctuations and phase. *Neuroscience*, 27(1), 289-300.

- [19] Schmidt, R. C., Turvey, M. T.: (1994) Phase-entrainment dynamics of visually coupled rhythmic movements. *Biological Cybernetics*, 70(4), 369–376.
- [20] Hart, Y., Noy L., Feniger-Schaal R., Mayo A.E., Alon U.: (2014) Individuality and Togetherness in Joint Improvised Motion. *PLoS ONE* 9(2): e87213. doi:10.1371/ journal.pone.0087213
- [21] Noy, L., Dekel, E., Alon, U.: (2011) The Mirror Game as a Paradigm for Studying the Dynamics of Two People Improvising Motion Together. *Proc Natl Acad Sci USA* 108:20947–20952.
- [22] Slowinski, P., Rooke, E., di Bernardo, M., Tsaneva-Atanasova, K.: (2014) Kinematic characteristics of motion in the mirror game. *IEEE International Conference on Systems, Man and Cybernetics*, 748–753.
- [23] Kullback, S., and Richard A. L.: (1951) On information and sufficiency. *The annals of mathematical statistics* 22(1):79-86.
- [24] Cohen, S., Guibas, L.: (1997) The earth mover’s distance: Lower bounds and invariance under translation. *DTIC Document*, Tech. Rep.
- [25] Levina, E., Bickel, P.: (2001) The earth mover’s distance is the mallows distance: some insights from statistics. 2001 Eighth IEEE International Conference on Computer Vision, ICCV 2001 Proceedings vol. 2, 251–256.
- [26] Muskulus, M., Verduyn-Lunel, S.: (2011) Wasserstein distances in the analysis of time series and dynamical systems. *Physica D: Nonlinear Phenomena*, Vol 240(1), 45–58.
- [27] Borg, I., Groenen, P.J.F.: (2005) *Modern Multidimensional Scaling: Theory and Applications*. Springer Series in Statistics 2nd ed. 2005, 614 p.
- [28] Noy, L., Alon, U., Friedman, J.: (2015) Corrective jitter motion shows similar individual frequencies for the arm and the finger. *Experimental Brain Research*, doi: 10.1007/s00221-015-4204-1
- [29] Chakravarty, I. M., Roy, J. D., and Laha, R. G.: (1967). *Handbook of Methods of Applied Statistics*, Volume I, John Wiley and Sons, pp. 392-394.
- [30] Noy, L., Binnun, N.L, Alon, U., Golland, Y.: (2015) Being in the zone: physiological markers of togetherness in joint improvisation. *Front. Hum. Neurosci*, doi: 10.3389/fnhum.2015.00187
- [31] Hogg, R. V., McKean, J., Craig, A. T.: (2005). *Introduction to mathematical statistics*. Pearson Education.

- [32] Issartel, J., Marin, L., and Cadopi, M.: *Unintended interpersonal coordination: “can we march to the beat of our own drum?”*. Neuroscience Letters 411, pp. 174–179 (2007)
- [33] (2015, March). [Online]. Available: <http://www.euromov.eu/alterego/>
- [34] (2015, March). [Online]. Available: <http://www.leapmotion.com>
- [35] Zhai, C., Alderisio, F., Tsaneva-Atanasova, K., di Bernardo, M.: (2014) Adaptive Tracking Control of a Virtual Player in the Mirror Game. Proceedings of IEEE Conference on Decision and Control (CDC), 7005–7010
- [36] Zhai, C., Alderisio, F., Tsaneva-Atanasova, K., di Bernardo, M.: (2014) A novel cognitive architecture for a human-like virtual player in the mirror game. Proceedings of IEEE International Conference on Systems, Man and Cybernetics (SMC), 754–759.
- [37] Kantorovich, L.V., Rubinstein, G.Sh.: (1958) On a space of completely additive functions (in Russian). Vestnik Leningrad Univ. 13(7), 52–59.
- [38] Varlet, M., Coey, C. A., Schmidt, R. C., Marin, L., Bardy, B. G., Richardson, M. J.: (2014) Influence of stimulus velocity profile on rhythmic visuomotor coordination. J Exp Psychol Hum Percept Perform, 40(5), 1849-1860
- [39] Kelso, J. S., de Guzman, G. C., Reveley, C., Tognoli, E.: (2009). Virtual partner interaction (VPI): exploring novel behaviors via coordination dynamics. PLoS One, 4(6), e5749.
- [40] Dumas, G., de Guzman, G. C., Tognoli, E., Kelso, J. S.: (2014). The human dynamic clamp as a paradigm for social interaction. Proceedings of the National Academy of Sciences, 111(35), E3726-E3734.
- [41] Billingsley, P.: Probability and Measure, Anniversary Edition. John Wiley and Sons, (2012)
- [42] Corder, G.W., Foreman, D.I.: (2014). Nonparametric Statistics: A Step-by-Step Approach. 2nd edition, Wiley.
- [43] Equis, S., Jacquot, P.: (2010) Phase Extraction in Dynamic Speckle Interferometry with Empirical Mode Decomposition and Hilbert Transform, Strain 46, 550–558
- [44] Fink, W.P., Kelso, S.J.A., Jirsa, V.K., de Guzman, G.: (2000) Recruitment of degrees of freedom stabilizes coordination. Journal of Experimental Psychology: Human Perception and Performance, 26(2), 671–692.

- [45] Fisher, N.I.: (1995) *Statistical Analysis of Circular Data*. Cambridge Univeristy Press, Cambridge, UK
- [46] Flash, T., Hogan, N.: (1985) The coordination of arm movements: an experimentally confirmed mathematical model. *J Neurosci* 5:1688–1703.
- [47] Grinsted, A, Moore, J.C., Jevrejeva, S.: (2004) Application of the cross wavelet transform and wavelet coherence to geophysical time series. *Nonlinear Processes in Geophysics* 11, 561–566
- [48] Issartel, J., Marin, L., Gaillot, P., Bardainne, T., Cadopi, M.: (2006). A practical guide on time-frequency analysis to study human motor behavior: the contribution of wavelet transform. *J. Mot. Behav.* 38, 139–159.
- [49] Issartel, J., Bardainne, T., Gaillot P., Marin L.: (2015) The relevance of the cross-wavelet transform in the analysis of human interaction: a tutorial. *Front. Psychol.* 5:1566.
- [50] Johnson, N.L., Kotz, S., Balakrishnan, N.: (1994) *Continuous Univariate Distributions, Volume 1*, Wiley-Interscience.
- [51] Kralemann, B., Cimponeriu, L., Rosenblum, M., Pikovsky, A., Mrowka, R.: (2008) Phase dynamics of coupled oscillators reconstructed from data. *Physical Review E*, 77(6), 066205.
- [52] Manly, B.F.: (2004) *Multivariate statistical methods: a primer*. CRC Press.
- [53] Marin, L., Bardy, B.G., Bootsma, R.J.: (1999) Level of gymnastic skill as an intrinsic constraint on postural coordination, *Journal of Sports Sciences*, 17:8, 615-626.
- [54] Pearson, K.: (1929) Editorial note to “Inequalities for moments of frequency functions and for various statistical constants”. *Biometrika* 21 (1–4), 370–375. doi:10.1093/biomet/21.1-4.361.
- [55] Revzen, S., Guckenheimer, J.M.: (2008) Estimating the phase of synchronized oscillators. *Physical Review E* 78, 051907.
- [56] Schmidt, R.C., Carello, C., Turvey, M.T.: (1990) Phase transitions and critical fluctuations in the visual coordination of rhythmic movements between people. *Journal of Experimental Psychology: Human Perception and Performance*, 16(2), 227–47.
- [57] Varlet, M., Richardson, M.J.: (2011) Computation of continuous relative phase and modulation of frequency of human movement. *Journal of biomechanics*, 44(6), 1200–1204.

[58] (2015, March). [Online]. Available: <http://www.stat.physik.uni-potsdam.de/mros/damoco2.html>

[59] (2015, March). [Online]. Available: <http://www.glaciology.net/wavelet-coherence>

4 Supplementary Information

Table 1: Human-avatar interaction, non-parametric correlations between $EMD(Ref, S)$ and $\mu RPE(L_a, F_h)$, $\sigma RPE(L_a, F_h)$, $\mu RPE(Ref, S)$ and $\sigma RPE(Ref, S)$. Relation between data is measured with Spearman’s rank correlation coefficient ρ and Kendall’s coefficient τ .

	$\mu RPE(L_a, F_h)$	p-value	$\sigma RPE(L_a, F_h)$	p-value
$EMD(Ref, S)$	$\rho=0.385,$ $\tau=0.252$	$p_\rho=5.2e-$ $05,$ $p_\tau=1.3e-$ 04	$\rho=0.342,$ $\tau=0.229$	$p_\rho=3.6e-$ $04, p_\tau=5e-$ 04
	$\mu RPE(Ref, S)$	p-value	$\sigma RPE(Ref, S)$	p-value
$EMD(Ref, S)$	$\rho=-0.005,$ $\tau=-0.017$	$p_\rho=0.9615,$ $p_\tau=0.7975$	$\rho=-0.036,$ $\tau=-0.035$	$p_\rho=0.7112,$ $p_\tau=0.5926$

4.1 Preprocessing

- In scenarios 1 and 3, position time series were interpolated with shape-preserving piecewise cubic interpolation (13Hz in experiment 1 and 40Hz in scenario 3).

Matlab command: `interp1(t, x, 0:1/Fs:t(end), 'pchip');` Fs is the sampling frequency, t is the series of time and x is the position time series.

- In scenarios 2 and 3, the position data was filtered with a zero-phase forward and reverse digital 2nd order lowpass (10Hz cut-off) Butterworth filter which is a maximally flat magnitude filter.

Matlab commands: `butter(2, 10/(Fs/2))` and `filtfilt`.

- The pre-processed position time series were used to estimate numerically their corresponding velocity time-series. To differentiate position time-series we used a forth-order finite difference scheme. We cut out the first and last 2 seconds of the signal. Furthermore, we limit velocities to 3.5 [a.u./s] in experiment 1 and to 2.7 [m/s] in scenarios 2 and

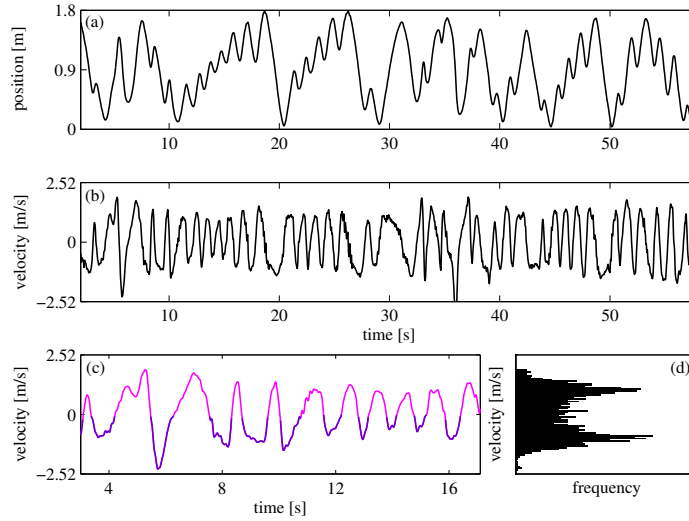


Figure 4: (a) An example of solo position time series from the Experiment 3. (b) Velocity estimated from position data. (c) Fragment of the velocity time series with indicated positive velocity segments (magenta) and negative velocity segments (purple). (d) Velocity profile - histogram of the velocity time series.

3 (higher velocities were considered a results of noise in the collected data).

- To estimate the PDF of the player’s velocity we use normalised histogram of the velocity time series with 101 equally distant bins between -2.7 and 2.7 [m/s] (or -3.5 and 3.5 [a.u./s] in Experiment 1).

Figure 4 illustrates initial stages of analysis of the data. Fig. 4 (a) depicts the representative player’s position collected in the solo condition in Scenario 3 and (b) its estimated velocity time-series as explained in *Materials and methods*. For each velocity time-series we compute velocity profile, which is the PDF of the player’s velocity time series. In Fig. 4 (d) we show the velocity profile of the time series represented in Fig. 4 (b). We use PDFs of velocity in order to capture the essence of the players’ movement without being affected by the existing physical constraints on their motion, e.g. limited position range. Multivariate distributions, involving consideration of more than one feature of the motion, would describe the dynamics in a more detailed way but we found that univariate distributions, namely of player’s velocities [5, 6, 2, 3, 4, 21, 20] contain enough information to achieve the goals of our study.

Finally, Figure 4 (c) depicts the first 20 seconds of the time series from Fig. 4 (b), with indicated positive velocity segments (magenta) for velocities

bigger than 0 that correspond to the movements of the hand from “left to right”, and negative velocity segments (purple) with velocities smaller than 0 that correspond to movements from “right to left”. To estimate the PDF of the player’s velocity we use normalised histogram of the velocity time series with 101 equally distant bins between -2.7 and 2.7 [m/s] (or -3.5 and 3.5 [a.u./s] in Experiment 1). In Fig. 4 (d) we show the velocity profile of the time series represented in Fig. 4 (b). In order to compare velocity profiles with velocity segments, for each velocity time-series from the experiments 1 and 3 we also find their velocity segments. Velocity segments are fragments of the velocity time series between two consecutive points of zero velocity, i.e. each velocity segments corresponds to a short movement in one direction. For our analysis, we normalise the velocity segments and compute their curve moments. Following [20, 21] we take into account only velocity segments that are longer than 0.2 sec., shorter than 8 sec. and which have displacement larger than 0.03 [m] (before normalisation). Note that, for the velocity segments, the moments of curve are computed with respect to time and hence parametrise the shape of the velocity segments rather than moments of the sample of velocity (see Section 4.4).

4.2 Earth’s movers distance

Mathematically the EMD is a special case of Wasserstein distance [25]. It is a solution of the optimal transportation problem [37] and is an established tool in image analysis and pattern recognition applications [25]. For univariate PDFs it can be expressed in a closed form as the area between their corresponding cumulative distribution functions [24]:

$$EMD(PDF_1(z), PDF_2(z)) = \int_Z |CDF_1(z) - CDF_2(z)| dz \quad (1)$$

Here, PDF_1 and PDF_2 are two probability density functions with support in set Z , CDF_1 and CDF_2 are their respective cumulative distribution functions. We note that EMD is a well-defined metric in the space of PDFs as it satisfies the following conditions:

Positive definiteness: $d(x_1, x_1) = 0, x_1 \neq x_2 \Rightarrow d(x_1, x_2) > 0,$

Symmetry: $d(x_1, x_2) = d(x_2, x_1),$

Triangle inequality: $d(x_1, x_2) \leq d(x_1, x_3) + d(x_2, x_3).$

These conditions express intuitive notions about the concept of distance. For example, that the distance between distinct points is positive and the distance from x to y is the same as the distance from y to x . The triangle inequality means that the distance from x to z via y is at least as great as from x to z directly. Furthermore, EMD is non-parametric and quantifies partial matches. Hence, it allows to compare PDFs rather than their selected moments. This represents a significant advantage of our analysis in

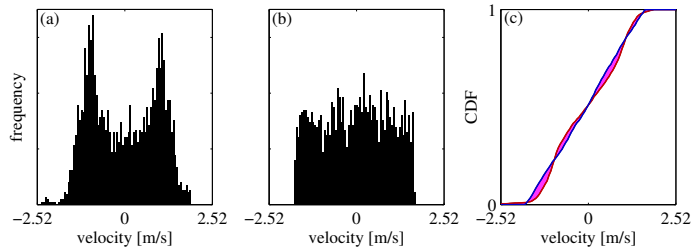


Figure 5: (a) Velocity profile - histogram (h_a) of the velocity time series. (b) Histogram (h_b) of a random variable generated with distribution of type-1 from the Pearson system. Both samples have $\mu = -0.01$, $\sigma = 0.54$, $s = -0.04$ and $k = 1.82$ where μ is the mean, σ is the standard deviation, s is the skewness and k is the kurtosis. (c) Cumulative density functions of the distribution from panel (a) in red and from panel (b) in blue. The magenta shading indicates the area of difference between the CDFs, i.e. the Earth's movers distance between the two distributions, $EMD(h_a, h_b) = 0.02$.

comparison to using selected moments, which are not sufficient to uniquely parameterise a PDF. We note that a bounded PDF is uniquely determined by its moments of all orders (0 to infinity) [41].

Figure 5 shows an example of two histograms with same estimates of the first four moments. The histogram in panel (a) is a velocity profile (h_a) computed for a time series in our data, while panel (b) shows a histogram (h_b) of random variable generated with distribution of type-1 from the Pearson system [50]; Matlab command: `pearsonpdf`. Figure 5 (c) demonstrates that by using the EMD we can distinguish between distributions which have the same first four moments; it also illustrates how the EDM between two experimental PDFs is computed. The red line in Fig. 5 (c) is the experimental CDF of the histogram from panel (a), while the blue line is the experimental CDF of the histogram from panel (b). The $EMD(h_a, h_b)$ between the two velocity profiles is the area between the red and the blue line, which is indicated with the magenta shading.

In practice, to compute empirical CDFs we take the cumulative sum of histogram bins normalised by the number of data points. We use histograms with 101 equidistant bins over fixed range of velocity values (outliers are assigned to the most extreme bins). Furthermore, we normalise the EMDs with the maximal EMD for a given support Z ; since $|CDF_1(z) - CDF_2(z)| \leq 1$, the maximal EMD is given by the length of the support $EMD_{max} = |Z|$. EMD can be computed using following Matlab code:

```

1 bins=linspace(z1,z2,101); % support Z with 101 bins
2 bin_width=bins(2)-bins(1); % widths of the bins, i.e. dz
3 max_emd=abs(z2-z1); % maximal EMD
4

```

```

5 h1=hist(v1,bins); % h1 and h2 are velocity profiles
6 h2=hist(v2,bins); % v1 and v2 are velocity time series
7 l1=numel(v1); % for normalisation
8 l2=numel(v2); % for normalisation
9 emd_v1v2=sum(abs(cumsum(h1/l1)-cumsum(h2/l2)))*bin_width/max_emd;

```

4.3 Multidimensional scaling

We use multidimensional scaling (MDS) to study relations between players' velocity profiles. MDS allows us to model the players' motion as points in an abstract geometric space, which we shall refer to as *similarity space*. It is a well established tool in data visualisation and data mining [27]. It allows to reduce dimensionality of the data and visualise relations between the objects under investigation while preserving as much information as possible. Since the EMD is a metric in the space of velocity profiles (defined by the PDFs of velocity time series), we use classical MDS as implemented in Matlab. We use the Matlab command: `cmdscale`.

In particular, we first compute the EMDs between all the analysed PDFs, which correspond to individuals' movements. Then we use the computed EMDs in order to construct a matrix \mathbf{D} . Each row of this matrix is assigned to a different PDF (and hence belongs to a specific individual, i.e. participant in the mirror game) and contains EMDs between this PDF and all the other PDFs. For instance, cell (2,3) contains the EMD between second and third PDFs in our dataset. Since the EMD is a metric, matrix \mathbf{D} has zeros on the diagonal and is symmetric.

Next, we use the MDS to transform matrix \mathbf{D} into coordinates of points in the *similarity space*. In this way each velocity profile is represented as a single point in the *similarity space*. Here we use only the first two dimensions of the *similarity space*, which were found to be sufficient for the purpose of our analysis. These two dimensions correspond to the first two highest eigenvalues of matrix \mathbf{D} computed in the MDS.

The MDS algorithm is implemented as follows:

1. Take $n \times n$ matrix \mathbf{D} (n number of analysed objects), and square its elements in order to obtain matrix \mathbf{D}^2 .
2. Transform matrix \mathbf{D}^2 into matrix \mathbf{B} ; subtract row means, subtract column means, add back (grand) mean of all the matrix elements and multiply by -0.5. Formally this operation is called double centring and can be expressed as: $\mathbf{B} = -0.5\mathbf{J}\mathbf{D}^2\mathbf{J}$, here $\mathbf{J} = \mathbf{I} - 1/n\mathbf{1}\mathbf{1}^T$, where \mathbf{I} is the identity matrix, $\mathbf{1}$ is the vector of ones of length n , and $\mathbf{1}^T$ is the transposed vector $\mathbf{1}$.
3. Factor \mathbf{B} by its eigendecomposition $\mathbf{B} = \mathbf{E}\mathbf{\Lambda}\mathbf{E}^T$, where \mathbf{E} is matrix which has eigenvectors of \mathbf{B} as columns, and $\mathbf{\Lambda}$ is a diagonal matrix with ordered eigenvalues $\lambda_1 \geq \lambda_2 \geq \dots \geq \lambda_n$ on the diagonal.

4. Take the first m eigenvectors \mathbf{E}_m and eigenvalues Λ_m of matrix \mathbf{B} and compute $\mathbf{X} = \mathbf{E}_m \Lambda_m^{1/2}$; \mathbf{X} is a $n \times m$ matrix with m coordinates for each of the n analysed objects; the MDS relies on the property that the eigenvectors of matrix $\mathbf{B} = \mathbf{X}\mathbf{X}^T$ can be interpreted as geometric coordinates; \mathbf{X}^T is transposed matrix \mathbf{X} .

MDS is a technique related to principal component analysis (PCA) [27]. In particular, PCA is a statistical procedure which uses singular value decomposition of a matrix \mathbf{Y} or eigendecomposition of covariance matrix $\mathbf{Y}^T\mathbf{Y}/(n-1)$ to study underlying structure of the data. Here \mathbf{Y} is a centred (i.e. its columns have removed means) $n \times m$ matrix of n observation vectors \tilde{Y} . In other words, the PCA uses the eigenvectors of the covariance matrix to perform orthonormal transformation of the original coordinate system of the data, i.e. it projects the data into an abstract geometric space with dimensions given by linear combinations of the the original variables. In the same way, the MDS uses eigenvectors and eigenvalues of matrix \mathbf{B} to find a geometric model of the data in an abstract geometric space. The difference between PCA and MDS is the origin and nature of the decomposed matrix. The results of both procedures are eigenvectors and eigenvalues which can be used to reduce the dimensionality of the data while preserving covariance of data (PCA) or preserving distances between analysed objects (MDS). In the case in which distances between analysed objects are given by covariances, i.e. $\mathbf{D} = 1 - \mathbf{Y}^T\mathbf{Y}$, or if \mathbf{D} is given by euclidian distances between n observations vectors \tilde{Y} , both methods give the same results.

The MDS allows us to extend pair-wise analysis of distances between velocity profiles and gain further insight into our data [22]. Furthermore, using MDS guarantees that the euclidian distances between elements in the *similarity space* are a good approximation of the EMDs between velocity profiles. Since EMD is a metric we know that the dynamic similarity between players' movements is reflected in the Euclidean distances between their respective positions in the *similarity space* (Fig. 1B, D), i.e. the closer the points in *similarity space* the more similar their velocity profiles. This renders the *similarity space* a key tool in our analysis of how the dynamic similarity affects mutual rapport and coordination between players in the mirror game. In the *similarity space* one can use different methods to classify and cluster data.

4.4 Moments of a curve

In Table 2 we recall the definitions of moments of curve.

In Table 2 $f(t)$ is a function defined on $T = [t_1, t_2]$.

To analyse and compare movements of different participants Noy et. al. use skewness and kurtosis of normalised velocity segments [20, 21]. To perform a meaningful comparison of the moments of different functions $f(t)$, it

Table 2: First 4 moments of function (curve) $f(t)$ with support $T=[t_1, t_2]$.

1st moment — centre of mass	$\mu = \int_{t_1}^{t_2} t f(t) dt$
2nd moment — variance	$\sigma = \int_{t_1}^{t_2} (t - \mu)^2 f(t) dt$
3rd moment — skewness	$s = \frac{1}{\sigma^2} \int_{t_1}^{t_2} (t - \mu)^3 f(t) dt$
4th moment — kurtosis	$k = \frac{1}{\sigma^2} \int_{t_1}^{t_2} (t - \mu)^4 f(t) dt$

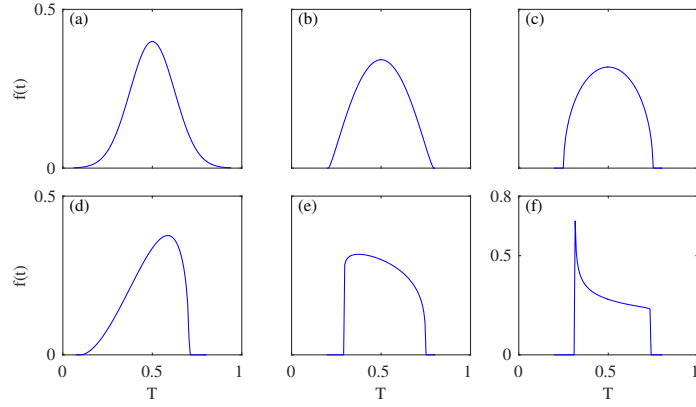


Figure 6: Different curve segments (a) Normal distribution $s = 0, k = 3$; (b) Minimum jerk $s = 0, k = 2.2$; (c) $s = 0, k = 2$; (d) $s = -0.5, k = 2.5$; (e) $s = 0.15, k = 1.9$; (f) $s = 0.2, k = 1.8$. For all distributions: $\mu = 0.5, \sigma = 1$.

is necessary to rescale their supports T to a common one, and to normalise the functions $f(t)$ with their integrals $\int_{t_1}^{t_2} f(t) dt$. In particular, in [21] as well as in our analysis the support T of the velocity segments is time normalised into $\tau \in [0, 1]$. We note that moments of curve are different from moments of a sample, i. e. they are computed with respect to the support, rather than the values in the sample. For example, in the case of the centre of mass, the area under the curve on the left side of the centre of mass μ is equal to the area under the curve on the right side of it, that is $\mu, \int_{t_1}^{\mu} f(t) dt = \int_{\mu}^{t_2} f(t) dt$.

Figure 6 depicts six examples of normalised curve segments with support $T \in [0, 1]$; all presented functions have the same centre of mass $\mu = 0.5$ and variance $\sigma = 1$, whilst skewness and kurtosis vary between panels. In the case of a velocity segment, skewness indicates asymmetry in acceleration

and deceleration, while kurtosis provides information about uniformity of the maximal velocity. Low kurtosis means that an object is quickly accelerating and decelerating and keeps constant velocity in between while high kurtosis means that the object is accelerating slowly, and after reaching maximum velocity it almost immediately starts to slow down; normalised velocity segments with higher kurtosis, generally, have higher maximum velocity.

4.5 Clustering, overlap and statistical tests

In order to analyse separation and clustering of data points corresponding to velocity profiles of individual participants in the *similarity space* or on the plane of skewness and kurtosis of velocity segments, we encircle them with ellipses given by bivariate gaussian distribution fitted to their coordinates. Then we compare how much the ellipses overlap.

First, we compute mean values and covariance matrix of coordinates of the n points which we wish to encircle. The points correspond to n trials of a particular subject. In particular, the coordinates are either average values of skewness and kurtosis of all the velocity segments in a trial, or coordinates of a point in the similarity space corresponding to a velocity profile of a trial. Mean values of the coordinates give the position of the centre of the ellipse, while the eigenvectors of the covariance matrix give directions of major and minor axes of the ellipse. Finally, the lengths of the axes of a covariance ellipse that encloses the desired probability mass are given by the square roots of the eigenvalues of the covariance matrix multiplied by the Mahalanobis radius [52]. In our analysis we use a radius that encloses all of the data points of a participant, which corresponds to 0.7 of the probability mass of the bivariate normal distribution.

We compute the overlap, ω , between ellipses as a ratio of the area of intersection and the total area of two ellipses. In this way total separation corresponds to no overlap $\omega = 0$, whilst complete overlap $\omega = 1$ means that we cannot distinguish between the two ellipses and hence we cannot distinguish between points that are encircled by them. The overlap ω between ellipses allows to assess clustering and separation between regions of the *similarity space*, or the plane of skewness and kurtosis of velocity segments, corresponding to different individuals. The advantage of this simple method is that it is dimension independent and hence allows to compare clustering and overlap in different spaces.

Since our data is not normally distributed, to test the existence of correlations we use Spearman's rank correlation coefficient ρ , and Kendall's coefficient τ [42]; the two rank correlation coefficients have different sensitivity to errors in ordering. To compute correlation coefficients and their significance values (p-values) we use Matlab commands: `[rho,p]=corr(x,y,'type','Spearman')` and `[ta,p]=corr(x,y,'type','Kendall')`. For the same reason, to test

statistical significance of differences between distributions we use Kolmogorov-Smirnov test computed with Matlab command `kstest2`. Kolmogorov-Smirnov test determines whether independent random samples are drawn from the same underlying continuous population [42].

4.6 Relative phase

Analysis of the relative phase between two (or more) oscillators is an established method for quantifying synchronisation (coordination) level and hence temporal correspondence between periodic time series [43, 57]. We performed such analysis by using a method of reconstructing phase of an oscillator from data as described in [51, 55]. In particular, following [51], we computed protophase using the Hilbert transform and transformed it into phase, which grows linearly with time, using the Damoco 2 toolbox for Matlab [58]. However, measures of temporal correspondence that rely on the relative phase based on the Hilbert transform are not suited for the analysis of the time series recorded in our experiments for the following reasons:

- they have non-zero local mean; signal with moving averages have big jumps in phases which introduce big errors in relative phase (see Fig. 2 in [43]),
- their amplitude and phase spectra are not well separated; relative phase is sensitive to changes of amplitude,
- in many cases the time series contain multiple frequencies; instantaneous phase based on the Hilbert transform can be computed but does not have a physical interpretation.

More information about issues stated in the above list and importance of different assumptions for correct estimation of the phase of a signal can be found in [43].

Since the results obtained from the analysis of relative phase based on Hilbert transform were not satisfactory, we decided to use a method of estimating the relative phase based on a wavelet transform of a time series [12, 48, 49]. In particular, we used estimation of relative phase based on wavelet coherence as described in [47] and implemented in Crosswavelet and Wavelet Coherence toolbox for Matlab [59]. Wavelet coherence can be considered a localised correlation coefficient in time-frequency space.

Wavelet coherence provided us with an estimate of relative phase in the time-frequency space, i.e. at each time we have multiple values of relative phase that correspond to different frequencies. To reduce dimensionality of the time frequency estimate of the relative phase, we averaged it over frequencies, obtaining in this way the time course of relative phase.

Figure 7 illustrates the process of averaging the estimate of the relative phase computed in the time-frequency space over frequency. In particular, Fig. 7 (a) shows the position time series of leader (black) and follower (green), while Fig. 7 (b1) shows the values of the wavelet coherence in the time-frequency space. Red colours indicate high coherence, i.e. the two signals have correlated frequency components at a given time, whilst blue ones indicate regions with no coherence. Black contour delineates the area where common frequencies of both signals are statistically significant; tested against random noise [47]. Arrows are a visualisation of the phase relation between correlated frequency components of the two time series (clockwise angles have negative values, anti-clockwise angles have positive values). Arrows pointing to the right show that the two signals are in-phase. For clarity only arrows in the regions with statistically significant coherence are shown.

Fig. 7 (b2) shows frequency average of relative phase ϕ_W from the regions with statistically significant coherence; we use circular mean to compute the average [45]. Fig. 7 (c) shows the relative phase based on the Hilbert transform ϕ_{prt} computed with the Damoco 2 toolbox [59]; multiple jumps in the relative phase are caused by the changes in the local means of the two signals. This figure clearly demonstrates that the estimate of the relative phase computed with wavelet coherence ϕ_W is better than the one based on Hilbert transform ϕ_{prt} , since the sign of the former is consistent with the fact that the designated leader was actually leading the other player during the joint action. The advantage of this method originates from the fact that ϕ_W is based on the parts of the signal which are measurably correlated and can be modelled with periodic functions in the time-frequency plane.

4.7 Relative position error

We introduce the *relative position error* (RPE) as a measure of position mismatch between leader and follower. In other words it is a measure of how well the follower tracks leader's movement. In particular, it informs us on the periods of time when the designated roles of leader and follower are exchanged. The RPE is an extension of position difference; it indeed measures the difference in position but in relation to the direction of players' movement.

The RPE is based on the notion that if two objects are moving in the same direction then the one behind is following, and on the assumption that changes of direction of movement are initiated by the leader. We define the RPE as the difference in the players' positions multiplied by their common direction of motion. In cases when the players are moving in opposite directions, we assume that the follower is always behind the leader, regardless of directions of players' movement. These rules lead to the following formula

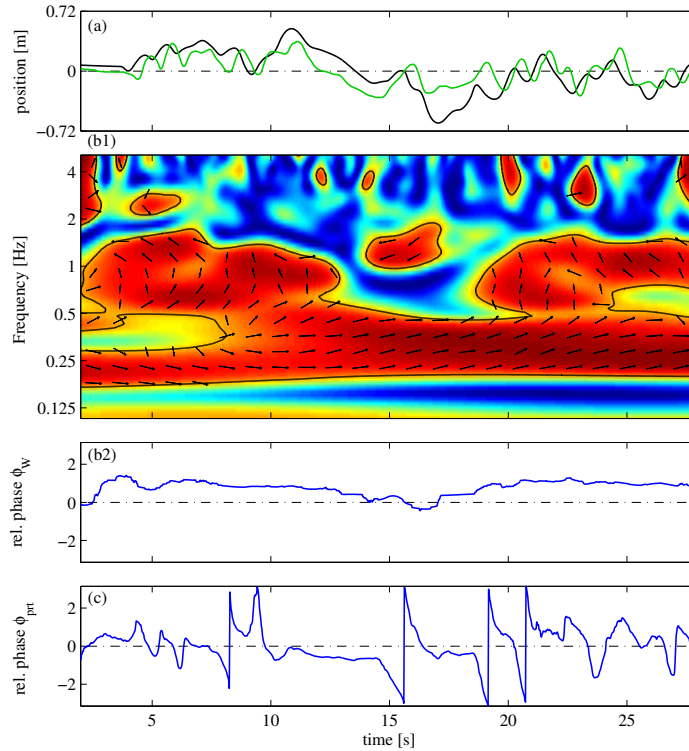


Figure 7: Relation between wavelet coherence and relative phase. (a) Position time series of leader (black) and follower (green). (b1) Squared wavelet coherence between leader and follower time series, red indicates high coherence and blue low coherence. Black contour shows 0.05 significance level, arrows indicate relative phase relationship (clockwise positive values, anti-clockwise negative values). (b2) Relative phase computed with significant wavelet coherence averaged over frequencies. (c) Relative phase between time series based on Hilbert transform.

for computing the $RPE(x_1, x_2)$:

$$RPE(x_1, x_2) = \begin{cases} (x_1(t) - x_2(t)) \operatorname{sgn}(v_1(t)), & \operatorname{sgn}(v_1(t)) = \operatorname{sgn}(v_2(t)) \neq 0, \\ |x_1(t) - x_2(t)|, & \text{otherwise.} \end{cases} \quad (2)$$

Here x_1, v_1 are position and velocity of the leader and x_2, v_2 are position and velocity of the follower. Positive values of the RPE mean that the follower is behind the leader. sgn is the signum function: $\operatorname{sgn}(x) = 1$, if $x > 0$, $\operatorname{sgn}(x) = 0$, if $x = 0$, and $\operatorname{sgn}(x) = -1$, if $x < 0$. Specifically, to compute the RPE we use signed difference in players position and their direction of movement, and this allows us to specify who is ahead in cases when both

players move to the left $\text{sgn}(v_1(t)) < 0$ or when they both move to the right $\text{sgn}(v_1(t)) > 0$. In cases where the notion of being ahead becomes ambiguous, because players move in opposite directions $\text{sgn}(v_1(t)) \neq \text{sgn}(v_2(t))$ or do not move at all, we use the absolute value of the difference in position. In our data we never encountered a case of $v_1(t) = v_2(t) = 0$, (recall that $\text{sgn}(0) = 0$). Note that the root mean square of the RPE will give exactly the same result as the root mean square error between two position time series. Furthermore, the RPE, similarly to the root mean square error, assumes that two time series (of motion) have a common coordinate system or can be transformed to it.

Figure 8 shows examples of computation of the RPE. Panels (a1) and (b1) depict trajectories of movement of two players, leader position is shown with black line, follower position is shown with green line; time flows from bottom to top. Fig. 8 (a2) and (b2) show corresponding time series of the RPE. Green arrows indicate the direction of motion of the follower. At the times indicated by double green-black arrows, when the participants move in opposite directions, we compute the RPE using the absolute value of the difference in position, i.e. we assume that the follower is always behind and that the leader initiates changes of direction of motion.

Figure 8 (a) shows how our definition of RPE works for the case when the players are often changing direction of motion. In panel (a2) we observe that the follower is always behind ($RPE > 0$) and that $RPE = 0$ occurs at times when the players had the same position but were moving in opposite directions. Fig. 8 (b) shows that if follower is ahead of the designated leader the RPE is negative. In such cases we can conclude that the designated leader was tracking the movement of the designated follower. Black-green arrows in Fig. 8 (b1) show that when the designated leader changed direction of movement, the RPE changed sign as well.

We note that the RPE is not symmetric, that is $RPE(x_1, x_2) \neq -RPE(x_1, x_2)$ (due to the assumption that a follower should react to the action of a leader) and therefore, it could be treated as a measure of the performance of the follower in addition to indicating the level of temporal correspondence (synchronization). Such interpretation of the RPE is consistent with the fact that the mismatch in position is one of the control parameters of the interactive cognitive architecture.

4.8 On the relation between temporal correspondence and dynamic similarity

When analysing two complex time-series, regardless of their origin, it is always possible to measure their temporal correspondence and compute their dynamic similarity. By using simultaneously these two quantities we can define trivial and nontrivial dynamic similarity.

More specifically, if the two time series are well synchronised, they will

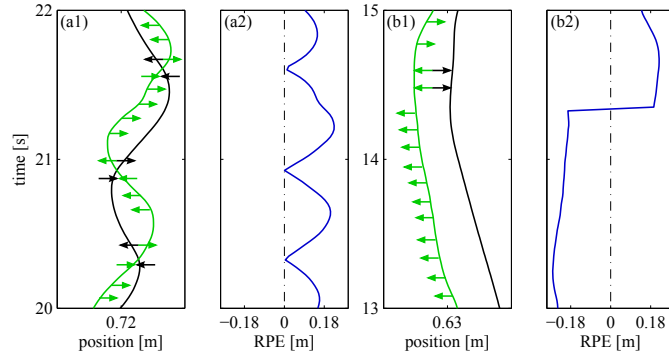


Figure 8: Illustration of the principle used for computing relative position error. In all panels: black is leader position, green is follower position, blue is relative position error. Green arrows show direction of motion of the follower. At the times indicated by double green-black arrows the participants move in opposite directions. Time runs from bottom to top.

necessarily have similar velocity profiles. For example, consider perfect synchronisation when two time series are identical, in such case also their velocity profiles have to be identical and the EMD between them equals 0, i.e. good coordination \Rightarrow small EMD. We shall call such dynamic similarity, which is a result of the coordination between time series, trivial. On the other hand, if the EMD between velocity profiles is small, while position time series are uncoordinated we observe nontrivial dynamic similarity i.e. small EMD $\not\Rightarrow$ good coordination level. Such situation is possible because velocity profiles do not contain temporal information. In particular, we use nontrivial dynamic similarity to establish existence of individual motor signature, and to show the dependence of temporal correspondence on the dynamic similarity.

Figure 9 illustrates the difference between trivial and nontrivial dynamic similarity. In panel (a) we show two trajectories of solo movement of a player and their corresponding velocity profiles. The mean RPE between the red and purple trajectories in panel (a1) is equal $\mu RPE_{a1}=0.19$, and the EMD between histograms in panels (a2) and (a3) is equal $EMD(h_{a2}, h_{a3})=0.009$; it is an example of nontrivial dynamic similarity. In panel (b) we depict leader (black) and follower (green) trajectories and their corresponding velocity profiles. Here: $RPE_{b1}=0.008$, and $EMD(h_{b2}, h_{b3})=0.008$; panel (b) shows example of trivial dynamic similarity.

4.9 Interpretation of dimensions of the *similarity space*

Here we elaborate on the relationship between dimensions of the *similarity space* and typical characteristics of complex movement, such as frequency components. The aim here is to demonstrate that although dimensions of

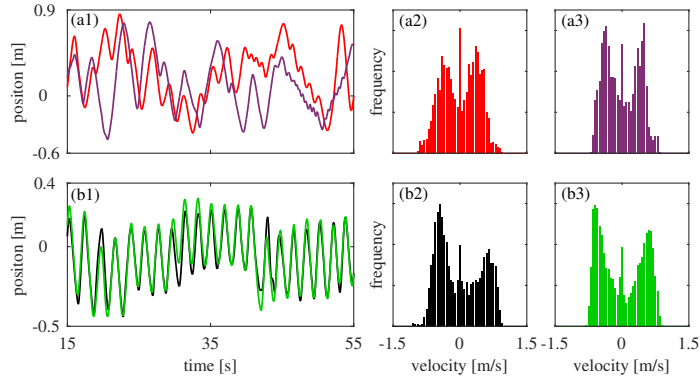


Figure 9: (a) Example of nontrivial dynamic similarity: (a1) two solo movement trajectories of the same participant and their corresponding velocity profiles (a2) and (a3); $RPE_{a1}=0.19$, $EMD(h_{a2}, h_{a3})=0.009$. (b) Example of trivial dynamic similarity: (b1) movement trajectories of a leader (black) and a follower (green) and corresponding velocity profiles (b2) and (b3); $RPE_{b1}=0.008$, $EMD(h_{b2}, h_{b3})=0.008$.

the *similarity space* are in general abstract, it is still possible to find movement characteristics that correlate with them, and give them at least partial physical interpretation. In general, possibility of physical interpretation should not be assumed, because as it happens in the PCA the dimensions of the *similarity space* might be linear combinations of many different characteristics of the analysed objects.

In the course of our analysis we identified two characteristics of the movements in the mirror game that correlate with the two principal dimensions of the *similarity space*: the coordinate x_{ss} and the coordinate y_{ss} . The coordinate x_{ss} of the *similarity space*, which is associated with the highest eigenvalue from the MDS, is correlated with the amount of high frequency components in the movement measured as a power in the 1.5-10 [Hz] band. In order to estimate the power spectrum of the position time series, we use the wavelet transform of the position time series summed over time. Since we are only interested in the frequencies, which belong to significant wavelets, the spectrum estimates computed in this way are smoother than the one computed with the fast Fourier transform (FFT). Furthermore, we found that the y_{ss} coordinate of the *similarity space*, associated with the second biggest eigenvalue from the MDS, is correlated with the kurtosis of velocity segments, described in Section 4.4. These correlations are illustrated in Fig. 10 and quantified in Table 3. Altogether these observations provide some interpretation of the dimensions in the abstract geometric space computed with the MDS. We note that such interpretation does not have to be unique, as there might exist other variables, or their linear combinations,

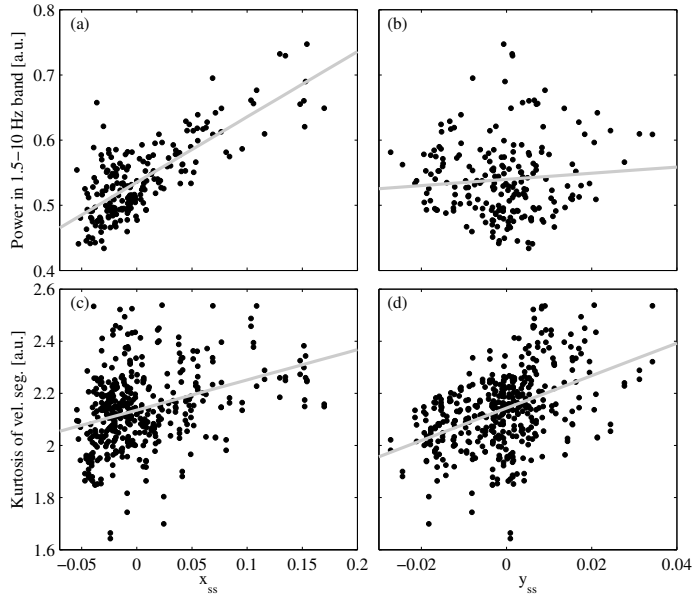


Figure 10: Dependencies: (a) between x_{ss} and power in the 1.5-10 [Hz] band, (b) between y_{ss} and power in the 1.5-10 [Hz] band, (c) between x_{ss} and kurtosis of velocity segments (positive and negative), and (d) between y_{ss} and kurtosis of velocity segments (positive and negative), for all solo trials recorded in the experiment. Grey line shows linear trend found with least square fitting. Trend is shown just for indication, relation between data has been tested with non-parametric correlations; see Tab. 3.

that correlate with x_{ss} or y_{ss} .

Figure 10 (b) and Table 3 show that there is no correlation between y_{ss} and power in the 1.5-10 [Hz] band and that the correlation between x_{ss} and kurtosis of velocity segments (panel (c)) is weaker compared to the other two. This indicates that x_{ss} is strongly related to the amount of high frequency components in the velocity time series and also weakly related to the kurtosis of velocity segments, and that y_{ss} is related to kurtosis of velocity segments. Correlation between high frequency components and kurtosis of velocity segments present in the data, means that they are not independent variables ($\rho=0.4412$, $p_\rho=2.2e-11$).

In summary, from the existing correlations we can deduce that x_{ss} carries information about maximal velocities; high kurtosis means that the velocity segment has sharper peak, that is higher maximal velocity, and high frequencies also mean faster movement. On the other hand, y_{ss} informs us on the ratio of high and low velocities in the movement; low kurtosis means that the player moves with maximal velocity for a long time, and high kurtosis means that the participant moves with maximal velocity only for a short

Table 3: Non-parametric correlations between x_{ss} and power in the 1.5-10 [Hz] band, y_{ss} and power in the 1.5-10 [Hz] band, x_{ss} and kurtosis of velocity segments (positive and negative), and y_{ss} and kurtosis of velocity segments (positive and negative), for all solo trials recorded in the experiment. The relationships between different characteristics of the movement is measured with Spearman’s rank correlation coefficient ρ and Kendall’s coefficient τ .

	x_{ss}	p-value	y_{ss}	p-value
power in 1.5-10 [Hz]	$\rho=0.6575,$ $\tau=0.4940$	$p_\rho=0,$ $p_\tau=1.0e-26$	$\rho=0.0183,$ $\tau=0.0055$	$p_\rho=0.79,$ $p_\tau=0.91$
Kurtosis of vel. seg.	$\rho=0.3566,$ $\tau=0.2407$	$p_\rho=3.7e-14,$ $p_\tau=1.4e-13$	$\rho=0.4576,$ $\tau=0.3180$	$p_\rho=2.5e-23,$ $p_\tau=1.5e-22$

period of time.

4.10 Velocity segments of movement generated by ICA

In this section we use kurtosis and skewness of velocity segments to show that the trajectories generated by the ICA [35, 36] in Scenario 3, have the features of a human movement. In our analysis we compared skewness and kurtosis of: velocity segments of human solo movement, velocity segments of human leader movements, and velocity segments of motion generated by the ICA as a leader. We found that except for few outliers, the velocity segments generated by the ICAv1.0 have the same kurtosis and skewness as the one observed in human motion.

Figure 11 shows kurtosis and skewness of velocity segments from time series recorded in experiment 3, (a) for positive velocity segments and (b) for negative velocity segments. The skewness and kurtosis of velocity segments from human solo is depicted in red, human leader in blue and avatar leader in black. We notice that for some very few outliers the skewness and kurtosis of the avatar leader (black) have bigger values than typical human leader (blue), but overall the black dots and blue circles occupy a similar region of the kurtosis-skewness plane. In both panels all the velocity segments are centred on the point with skewness $s = 0$, and kurtosis $k = 2.2$, which is indicated by a cyan star. This point corresponds to the velocity segment with the smoothest movement as reported in [20, 21]. Normal distribution has skewness $s = 0$, and kurtosis $k = 3$. Dash-dotted line shows theoretical bound of the values of skewness and kurtosis given by the theoretical relation between them $k \leq s^2 + 1$ [54].

In Table 4 we report the difference in skewness of the positive and neg-

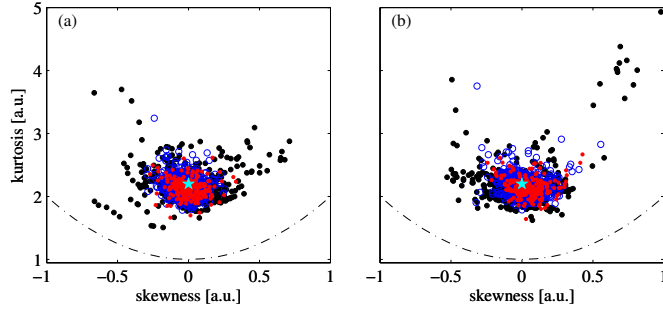


Figure 11: Kurtosis and skewness for velocity segments from time series recorded in the experiment. In panel (a) values from positive velocity segments, in (b) from negative velocity segments; compare with Fig. 4 (c). In black skewness and kurtosis of velocity segments from ICA in leader conditions. In blue skewness and kurtosis of velocity segments from human players in leader conditions. In red skewness and kurtosis of velocity segments from human players in solo conditions. Cyan star indicates point with $k = 2.2$ and $s = 0$ which corresponds to the smoothest movement [20]. Dash-dotted line shows theoretical bound given by relation between kurtosis and skewness of a curve $k \leq s^2 + 1$ [54].

ative velocity segments. This difference is a result of asymmetry in the movement of the hand towards and away from the centre of the body, i.e., the movement is actuated by different groups of muscles [46]. Relatively weaker difference in skewness of the positive and negative velocity segments of avatar leader is due to the fact that, while leading the human follower, the avatar was at the same time tracking the pre-recorded reference trajectory. Furthermore, we observe that human followers' velocity segments are equally skewed for positive and negative velocity segments. We have not found difference between kurtosis of positive and negative velocity segments in any condition.

Table 4: Skewness of positive s_+ and negative s_- velocity segments from different movement recordings: S - human solo movement, L_h - human leader, F_a - avatar follower, L_a - avatar leader, F_h - human follower. p_{ks} is significance level of Kolmogorov-Smirnov test.

	s_+	s_-	p-value
S	0.0018	0.0456	$p_{ks}=3.9e-4$
L_h	-0.0147	0.0238	$p_{ks} < 0.0001$
L_a	0.0065	0.0143	$p_{ks}=0.0781$
F_h	0.1300	0.1267	$p_{ks}=0.1653$

In summary, Fig. 11 shows that in most trials, velocity segments of the avatar leader (driven by ICA v1.0) have kurtosis and skewness which are very similar to the human players. Furthermore, the values of skewness of the human follower’s velocity segments are consistent with the observation that after noticing changes of direction of the leader’s movement, the human follower reacts and accelerates quickly to correct her/his position. Next, she/he slows down to track the leader’s movement in a more precise way.

4.11 Comparison of different measures of temporal correspondence

Having introduced different measures of temporal correspondence in the sections above we now compare the relative error in position and the estimate of the relative phase based on wavelet coherence, using data from experiment 3 (we used data from experiment 3 because it contains the largest number of trials).

Figure 12 (a) shows position time series of leader (black) and follower (green) (the plots do not start from zero because we cut out the first 2 seconds of the signals). Fig. 12 (b) shows the RPE between the positions in panel (a), while Fig. 12 (c) shows the estimate of relative phase based on the wavelets coherence. We observe in Fig. 12 (b) and (c) that the RPE behaves differently compared to the relative phase, e.g. in the time interval [10,15] the RPE indicates that the follower is ahead of the leader ($RPE < 0$), while the relative phase shows that there was no exchange of roles between leader and follower. This different behaviour is caused by the fact that the RPE is computed using the information at a given instant of time, while the estimate of the relative phase is based on the wavelet transformation for which time localisation depends on the frequency and is limited by the time-frequency uncertainty principle [47]. Also, in this time interval there are no fast oscillations in the movement, therefore the phase was estimated using low frequency wavelets for which the relative phase was positive (compare with Fig. 7 (b)).

The negative value of the relative phase in Fig. 12 (c) around $t = 17s$ is caused by the temporal mismatch between the minimum in the follower’s trajectory (green) and the next minimum on the leader’s trajectory (black). The minimum in the leader’s trajectory indicated by the vertical dotted line in panel (a) occurs after the green one, while all the other extrema of the black trace precede the green trace extrema. The relatively fast change in trajectory in this case was estimated by using higher frequency wavelet of short duration for which the relative phase was negative. Observations from Fig. 12 (c) are consistent with the RPE in panel (b) which has negative values for a short time around $t = 17s$.

We further used data from Scenario 3 to compare the two methods of measuring temporal correspondence. Specifically, we computed RPE and

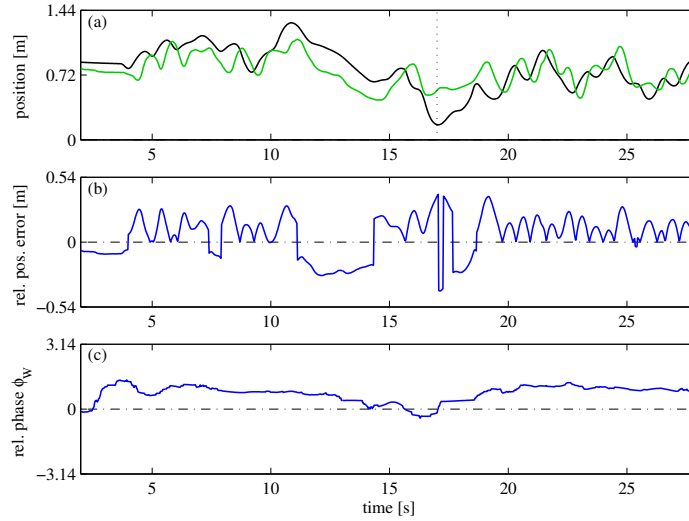


Figure 12: Comparison of relative position error and relative phase computed with wavelet coherence. (a) position time series of leader (black) and follower (green). (b) Relative position error. (c) Relative phase computed with wavelet coherence ϕ_W .

relative phase for leader–follower data, to analyse dependence of temporal correspondence on power content in the 1.5-10 [Hz] frequency band of the leaders position time series and on the first coordinate, x_{ss} , of the point corresponding to the leader’s velocity profile in the *similarity space*, which is correlated with power content in the 1.5-10 [Hz] frequency band, see section 4.9. In particular, we found that in contrast to relative phase, the RPE allows to quantify the level of coordination of two complicated time series and can be used to evidence that the temporal correspondence is significantly affected by the properties of leader’s motion.

In Fig. 13 we demonstrate that in our data we do not observe dependence of the relative phase ϕ_W between avatar-leader and human-follower (estimated with wavelet coherence) on x_{ss} nor on the power spectrum in the 1.5-10 [Hz] band of the leader’s position time series; since the relative phase is a circular variable in the analysis we use circular mean and circular standard deviation [45]. We believe that the lack of such dependence in our data is caused by the deficiencies of relative phase as a method of measuring temporal correspondence between aperiodic time series rather than by the real lack of it. Therefore, we checked whether the RPE between avatar-leader and human-follower depends on the coordinates of velocity profiles of avatar-leader in the *similarity space* or on the power in the 1.5-10 [Hz] frequency band.

We found that, while the mean of the relative position error $\mu RPE(L_a, F_h)$

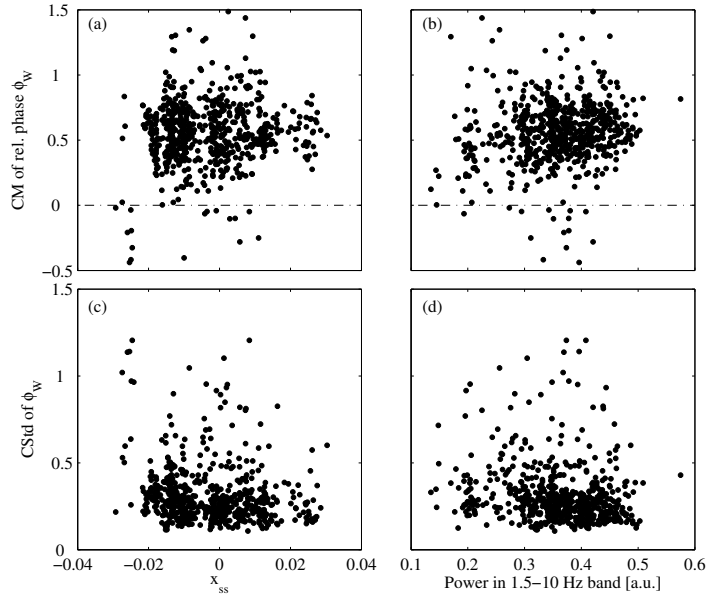


Figure 13: Dependencies: (a) between x_{ss} and circular mean of relative phase ϕ_W , (b) between power in the 1.5-10 [Hz] band and circular mean of relative phase ϕ_W , (c) between x_{ss} and circular standard deviation of relative phase ϕ_W , and (d) between power in the 1.5-10 [Hz] band and circular standard deviation of the relative phase ϕ_W . Relative phase ϕ_W computed for the avatar leader/ human follower condition recorded in the experiment. There are no significant correlations in the data.

depends on x_{ss} as well as on the power in the 1.5-10 [Hz] band of the power spectrum of the leader motion, the standard deviation $\sigma RPE(L_a, F_h)$ depends only on x_{ss} . Figure 14 and Table 5 show that the increase in the mean RPE is correlated with x_{ss} , and can also be associated with the higher number of high frequency components in the leader trajectory. On the other hand, the standard deviation of the RPE is only correlated with x_{ss} ; there is no correlation with the power in the 1.5-10 [Hz] band. Additionally, Table 5 shows that mean and standard deviation of RPE depend on y_{ss} .

The strong correlations of mean μ and standard deviation σ of the RPE with the principle (main) dimensions of the *similarity space* presented in Tab. 5 indicate that temporal correspondence depends on the dynamics of the movements, and could be represented by the location in the *similarity space*. Our results related to the dependence of temporal correspondence between complex non-periodic movements on spectral properties of the motion are consistent with earlier findings which showed existence of relation between standard deviation of the relative phase (or the relative phase itself) and common frequency of coupled oscillators [44, 53, 56]. This relation

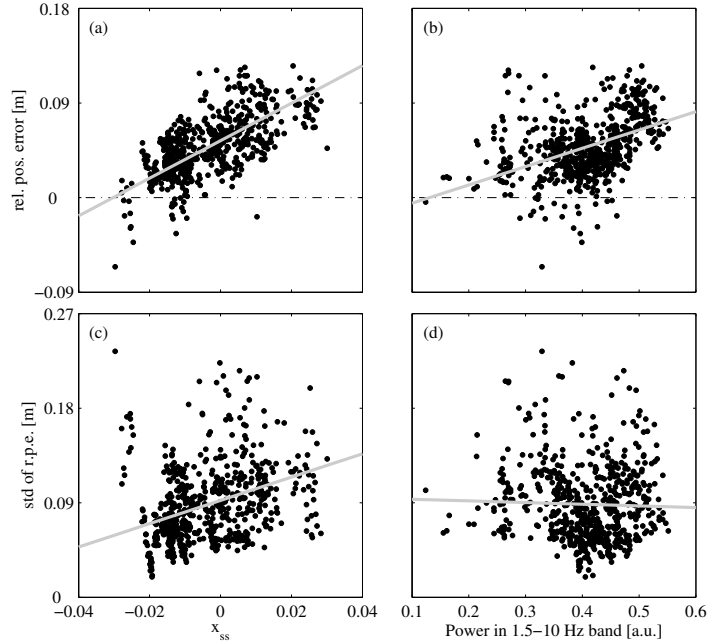


Figure 14: Dependencies: (a) between x_{ss} and the mean of the RPE, (b) between the power in the 1.5-10 [Hz] band and the mean of the RPE, (c) between x_{ss} and the standard deviation of the RPE, and (d) between the power in the 1.5-10 [Hz] band and the standard deviation of the RPE. The RPE is computed for the avatar leader human follower condition recorded in the experiment. Grey line shows linear trend found with least square fitting. Trend is shown just for indication, relation between data has been tested with non-parametric correlations, see Tab. 5.

was used to show the dependence of stability of coordination observed in synchronised movements (measured with standard deviation of the relative phase) on the frequency of movements [53]. In our case the stability of coordination (measured with the standard deviation of the RPE) is associated with (depends on) the location of the leader’s velocity profile in the *similarity space*.

More generally, based on our analysis and the example discussed above, we conclude that in the context of the mirror game, where the players move along complicated trajectories, the most useful method for quantification and assessment of the leader-follower interaction is the RPE measure. Specifically, the RPE exhibits stronger association to the dynamics of the movement (in terms of statistical significance of the results of the analysis), than the relative phase. Nevertheless, we envisage that the relative phase based on wavelet coherence would be useful when analysing data from the

Table 5: Non-parametric correlations between: x_{ss} or y_{ss} and the mean RPE, the power in the 1.5-10 [Hz] band and the mean RPE, x_{ss} or y_{ss} and the standard deviation of RPE, and the power in the 1.5-10 [Hz] and the standard deviation of the RPE. The RPE is computed for the avatar leader human follower condition recorded in the experiment. Relation between data is measured with Spearman’s rank correlation coefficient ρ and Kendall’s coefficient τ .

	mean RPE	p-value	std of RPE	p-value
x_{ss}	$\rho=0.6633,$ $\tau=0.4698$	$p_\rho=0,$ $p_\tau < 0.0001$	$\rho=0.3578,$ $\tau=0.2443$	$p_\rho=0,$ $p_\tau < 0.0001$
y_{ss}	$\rho=-0.2794,$ $\tau=-0.1990$	$p_\rho < 0.0001,$ $p_\tau < 0.0001$	$\rho=0.1911,$ $\tau=0.1284$	$p_\rho < 0.0001,$ $p_\tau < 0.0001$
power in 1.5-10 [Hz]	$\rho=0.4304,$ $\tau=0.2937$	$p_\rho=0,$ $p_\tau < 0.0001$	$\rho=-0.0460,$ $\tau=-0.0361$	$p_\rho=0.25,$ $p_\tau=0.17$

mirror game played in a condition without designated leader, e.g. joint improvisation, when the RPE cannot be used. Finally, an advantage of using the RPE to quantify temporal correspondence is its straightforward physical interpretation.